AGU ADVANCING EARTH AND SPACE SCIENCES

JGR Space Physics

RESEARCH ARTICLE
10.1029/2023JA032057

Key Points:

- Intense storms contain two types of recovery morphology, with a dominant two-stage recovery type of 60%
- Southward IMF plays a key role in the recovery phase morphology, and the Alfvén wave is an important interplanetary origin
- Average IMF B_Z of the continuous Alfvén wave positively affects the recovery rate in the later recovery phase

Correspondence to:
H. Li,
hli@spaceweather.ac.cn

Citation:
Li, H., Liu, X., & Wang, C. (2024). How solar wind controls the recovery phase morphology of intense magnetic storms. *Journal of Geophysical Research: Space Physics*, *129*, e2023JA032057. https://doi.org/10.1029/2023JA032057

Received 9 SEP 2023
Accepted 13 FEB 2024

Author Contributions:
Conceptualization: Hui Li, Chi Wang
Data curation: Xiaodong Liu
Formal analysis: Hui Li, Xiaodong Liu
Funding acquisition: Hui Li, Chi Wang
Investigation: Hui Li, Xiaodong Liu, Chi Wang
Methodology: Hui Li, Xiaodong Liu
Project administration: Hui Li, Chi Wang
Resources: Chi Wang
Software: Xiaodong Liu
Supervision: Hui Li
Validation: Hui Li
Visualization: Xiaodong Liu
Writing – original draft: Hui Li, Xiaodong Liu
Writing – review & editing: Hui Li, Chi Wang

How Solar Wind Controls the Recovery Phase Morphology of Intense Magnetic Storms

Hui Li[1,2,3], Xiaodong Liu[1,2,3], and Chi Wang[1,2,3]

[1]State Key Laboratory of Space Weather, National Space Science Center, CAS, Beijing, China, [2]Key Laboratory of Solar Activity and Space Weather, National Space Science Center, CAS, Beijing, China, [3]University of Chinese Academy of Sciences, Beijing, China

Abstract Geomagnetic storms are critical space weather phenomena resulting from the interaction between the solar wind and the Earth's magnetosphere. However, most studies focus on the main phase of magnetic storms, leaving the morphology of the recovery phase an open question. In this study, we analyze 82 intense magnetic storms with the minimum *Dst* index ≤ -100 nT between 1995 and 2018, finding that these storms can be classified into two distinct types: one-stage recovery storms that exhibit a single rapid exponential recovery and two-stage recovery storms that are characterized by a rapid exponential recovery in the early recovery phase and a slow linear recovery in the later recovery phase. We find that the two-stage recovery storms are dominant, accounting for approximately 60% of the events. Interestingly, the proportion of two-stage recovery storms peaks during solar minimum. The two-stage recovery storms tend to be accompanied by more Alfvén waves with long-duration and intense southward interplanetary magnetic fields. In addition, we find that the decay rate of the *Dst* index in the later recovery phase is correlated with the average B_Z of the interplanetary magnetic field when the solar wind has a high degree of Alfvénicity. Overall, our results shed new light on the recovery phase morphology of intense magnetic storms and highlight the role of Alfvén waves in this process.

Plain Language Summary Geomagnetic storms are severe space weather phenomena that can cause significant impacts on our technological infrastructure. Compared to the main phase, rare emphasis has been paid to the recovery phase. However, considering the long duration, understanding the storm recovery phase is essential to predict when the effects of space weather will subside. In this study, we analyzed 82 intense magnetic storms with the minimum *Dst* index ≤ -100 nT during the last two solar cycles, focusing on the statistical characteristics of the recovery phase morphology. These intense storms can be categorized into two distinct types: one-stage recovery storms with a rapid exponential recovery, two-stage recovery storms with a rapid exponential recovery in the early recovery phase, and a slow linear recovery in the later recovery phase. In addition, two-stage recovery storms are dominant and often accompanied by long-duration Alfvén waves with intense southward interplanetary magnetic fields. The decay rate of the *Dst* index in the later recovery phase correlates with the strength of the southward magnetic field when the solar wind presents a high degree of Alfvénicity. Our findings provide new insights into the recovery phase of intense magnetic storms and highlight the significance of Alfvén waves in this process.

1. Introduction

Geomagnetic storms are severe global phenomena that can significantly impact high-tech systems, such as communication, navigation, power grids, and satellites. Consequently, geomagnetic storms have become a hot issue of space weather research in the literature (Gonzalez et al., 1994, 1999). During a geomagnetic storm, the horizontal component of the geomagnetic field undergoes the most significant change and is the most reliable representation of the geomagnetic storm process. Thus, the *Dst* index is widely used to represent the average variation of the horizontal component of the Earth's magnetic field at low- and mid-latitudes and describe the evolution of magnetic storms.

Typical geomagnetic storms can be divided into three phases based on changes in the *Dst* index: the initial phase, the main phase, and the recovery phase. During the initial phase, the *Dst* index presents an enhancement from the prestorm level due to the compression of the magnetosphere by interplanetary disturbances. The main phase is characterized by a sudden decrease in the *Dst* index to its minimum value, which is used to define the intensity of the storm. Finally, the recovery phase begins as the *Dst* index gradually returns to the prestorm level. Statistically, for intense storms with the minimum *Dst* index ≤ -100 nT, the duration of the recovery phase is 58.4 hr, which is much longer than that of the main phase, 14.0 hr (Yokoyama & Kamide, 1997). Therefore, characterizing the morphology of the recovery phase and identifying the corresponding impact factors in the solar wind is crucial to understanding the evolution of geomagnetic storms and mitigating their potential impact on technological systems.

The magnetic storm recovery phase is of great significance in space weather research. For example, the magnitude of the spacecraft potential is, on average, significantly elevated for a longer period during the recovery phase than during the main phase (Denton et al., 2006). The day-side ionospheric equatorial electric field shows persistent eastward enhancement, and the occurrence of enhancement is higher in the second to fourth days of the recovery phase (Lei et al., 2018; Li et al., 2022). Sudden increases in the AE index and geomagnetically induced current bursts (GICs) in power lines also occur frequently during the storm recovery phase, and a very long recovery phase causes long-lasting GICs (Khanal et al., 2019; Kozyreva et al., 2018).

Direct studies on the recovery phase morphology of magnetic storms are very rare. Early investigations of recovery phases focused primarily on their duration. There exist two primary drivers of magnetic storms, namely interplanetary coronal mass ejections (ICMEs) and corotating interaction regions (CIRs). Generally, ICME-driven magnetic storms exhibit higher intensity and shorter duration of the recovery phase, whereas those induced by CIRs exhibit lower intensity and longer duration of the recovery phase. Furthermore, the duration of the recovery phase for CIR-driven magnetic storms shows a noticeable correlation with the duration of the main phase, whereas no such correlation is apparent for ICME-driven magnetic storms (Yermolaev et al., 2014).

In addition to the duration of the recovery phase, mathematical models of the *Dst* index during the recovery phase and the corresponding physical interpretation also attract many concerns. Without considering the energy input, the *Dst* index can be modeled as an exponential function (Dessler & Parker, 1959). When considering the energy input, the *Dst* index can be modeled as a hyperbolic function (Aguado et al., 2010). Later on, some studies showed that the recovery phase has two stages, with a first rapid recovery followed by a slower recovery. A proposed explanation for such a two-stage recovery is the existence of two spatially separated ring current populations (Akasofu et al., 1963). During intense storms, the ring current has both inner and outer components, with the inner component decaying more rapidly. Hamilton et al. (1988) attributed this phenomenon to the presence of two different ion components, H^+ and O^+, in the ring current. The decay time of H^+ is much longer than that of O^+. Furthermore, Feldstein et al. (2000) suggested that the decay of the *Dst* index during the recovery phase is controlled by two different magnetospheric current systems: the ring current and the magneto-tail current. In the early stage of the recovery phase, the drift loss of partial ring current at the dayside magnetopause dominates the decay of the *Dst* index. Afterward, the charge exchange of symmetric ring current becomes more significant (Liemohn et al., 1999).

Recently, growing concerns are paid to the role of Alfvén waves (AWs) in the recovery phase of extreme geomagnetic storms caused by ICMEs. Raghav et al. (2019) demonstrated that such storms exhibit a much longer two-stage recovery phase than expected, and attributed this to AWs. They proposed a combination of an exponential function and a linear function to describe the two-stage recovery phase. Based on a statistical survey, Telloni et al. (2021) found a high correlation between the duration of Alfvénic streams and the concurrent recovery phases. AWs are considered as an important source of long-duration southward interplanetary magnetic field (IMF) in the solar wind, which is a strong driver of geomagnetic activity (Zhang et al., 2014). It has also been shown that interplanetary AWs can cause intense geomagnetic aurora activity, known as High Intensity Long Duration Continuous AE Activity (HILDCAA) events (Tsurutani & Gonzalez, 1987). The study revealed that the AE index is affected not only by the presence of Alfvénic fluctuations but also by the magnitude of these fluctuations. However, no such statistical correlation was observed between solar wind turbulence and the geomagnetic response at low latitudes (D'Amicis et al., 2020).

The recovery phase of geomagnetic storms is a complicated process that depends on both the decay of the current system in the magnetosphere and interplanetary conditions. Previous studies have indicated that interplanetary AWs play an irrespective role in affecting the recovery phase. However, so far, no statistical investigation of the relationship between AW parameters and the recovery rate of magnetic storms has been conducted. The primary objective of this work is to investigate the morphology of the recovery phase and its dependence on the IMF and AWs conditions by conducting a statistical survey on intense storms.

2. Methodology

To begin our investigation, we first identify isolated intense magnetic storms that occurred between April 1995 and January 2020. Subsequently, we classify these storms into two distinct categories based on their recovery phase morphology, namely one-stage recovery storms and two-stage recovery storms. Finally, we explore the potential relationship between the recovery phase morphology and the solar wind conditions, including the presence of AWs.

2.1. Identify Isolated Intense Magnetic Storms

In this study, we mainly investigate the statistical characteristics of isolated intense storms. An isolated intense storm satisfies two criteria: (a) the minimum *Dst* index is less than −100 nT and (b) no moderate storm occurs until the preceding storm has fully recovered. Using these criteria, we identify 82 isolated intense storms for analysis. To eliminate interference from the dayside magnetopause current, we utilize the pressure-corrected index, Dst_c, in our subsequent analysis, which is obtained from the following formula proposed by Burton et al. (1975):

$$Dst_c = Dst + b \times \sqrt{P_d} + c \tag{1}$$

where P_d is the dynamic pressure of the solar wind. The coefficients b and c have been proposed according to different models, but the differences are not significant. Here, we choose $b = 7.26$ nT·nPa$^{1/2}$ and $c = 11.0$ nT (O'Brien & McPherron, 2000).

2.2. Classify Recovery Phase Morphology

For each isolated intense storm, the recovery phase is defined as the time interval from the minimum *Dst* index to the time the *Dst* index recovers to −20 nT. The classification technique for the morphology of the recovery phase is summarized as follows:

1. We fit the Dst_c index throughout the recovery phase by using a single exponential function and obtain the fitting goodness, R1, which is given by the following formula:

$$R1 = 1 - \frac{\sum\left(Dst_c - Dst_c'\right)^2}{\sum\left(\overline{Dst_c} - Dst_c\right)^2} \tag{2}$$

   where Dst_c' is the fitting data of Dst_c, and $\overline{Dst_c}$ is the mean value of Dst_c.

2. For some storms, the early rapid exponential recovery phase is much shorter than the later linear recovery phase. Although there are two different recovery patterns, R1 is quite close to 1 as well. Thus, we introduce another parameter to perform a better classification. We fit the Dst_c index throughout the recovery phase by using a piece-wise function, which includes an exponential function for the early recovery phase, and a linear function for the later recovery phase. A similar fitting approach has been used in previous studies (Choraghe et al., 2021; Raghav & Kule, 2018). By changing the separation point of these two functions, we identify the best-fitting break-point by making the overall fitting error at the lowest level. Then we extend the exponential function in the first stage to the end of the recovery phase and obtain the corresponding fitting goodness, R2, which is calculated in the same way as R1.
3. With both $R1 > 0.9$ and $R2 > 0.8$, such a magnetic storm can be classified as a one-stage recovery storm; otherwise, it is classified as a two-stage recovery storm. Note that these two threshold values are determined by practice. We also change these two values without finding significant changes in the results. For two-stage recovery storms, the interval preceding the break-point is denoted as the early recovery phase, while the period after the break-point is denoted as the later recovery phase.

Statistically, the Dst_c index has recovered by 63% at the break-point of two-stage recovery storms. To allow comparison of these two types of storms in the later recovery phase, we artificially set the break-point when the Dst_c index has been recovered by 63% for one-stage recovery storms. The first stage is defined as the early recovery phase, and the second stage is defined as the later recovery phase.

2.3. Identify Alfvén Waves

We use solar wind plasma and magnetic field data in geocentric solar magnetospheric (GSM) coordinates from the Wind spacecraft to analyze the interplanetary conditions during the geomagnetic storm recovery phase, and apply the approach proposed by Li et al. (2016) to identify AWs:

$$\delta V_i = \pm \delta V_{Ai} \tag{3}$$

where δV_i and δV_{Ai} are the band-pass filtered data of solar wind velocity V and Alfvén velocity V_A in 10 even logarithmic periods channel from 10 s to 1,000 s. The ± represents the direction of wave propagation parallel or anti-parallel to the background magnetic field. Li et al. (2016) also proposed a parameter to evaluate the Alfvénicity:

$$E_{rr} = \frac{1}{8}\left[||\gamma_c| - 1| + \sum ||\gamma_{ci}| - 1| + \left| \frac{\sigma_{\delta V}}{\sigma_{\delta V_A}} - 1 \right| + \sum \left| \frac{\sigma_{\delta V_i}}{\sigma_{\delta V_{Ai}}} - 1 \right| \right] \quad (i = x, y, z) \tag{4}$$

where γ_c is the correlation coefficient between δV_i and δV_{Ai}, σ is the standard deviation. The AWs are purer when the Err is closer to 0. The intervals with $Err \le 0.3$ for more than three channels are considered as AWs in this study.

3. Result

3.1. Case Study

The isolated magnetic storms analyzed in this study exhibit various recovery phase morphology and associated AWs. Four typical storm cases with different characteristics are presented in Figure 1, that is, one-stage recovery storms with/without AWs and two-stage recovery storms with/without AWs. In the upper panel of each case, the Dst_c index and its corresponding curve fitting during the recovery phase are shown. For one-stage recovery storms, the green line represents the fit of a single exponential function. For two-stage recovery storms, the red line represents the exponential function fitting for the early recovery phase, and the blue line represents the linear function fitting for the later recovery phase. The red dashed line is the extension of the red line and is used to calculate R2. The middle panel shows the diagnosis results of AWs. All the regions in color indicate the presence of AWs, and the regions in blue represent the presence of relatively pure AWs. The bottom panel displays the IMF B_Z in GSM coordinates, as observed by the Wind satellite, and the two vertical lines denote the recovery phase interval.

Figure 1a presents a one-stage recovery storm that occurred during 3–4 April 2004, with rapid recovery without AW. The Dst_c index is well-described by an exponential fitting, with R1 of 0.94 and a low root-mean-square error (RMSE) of 6.85 nT. The storm recovered from −100 to −20 nT in a short period of only 14 hr. During the recovery phase, the IMF B_Z was predominantly northward, with an average value of 6.38 nT. In addition, no clear AWs are observed. In contrast, Figure 1b displays a one-stage recovery storm that occurred on 24–27 July 2004, with long-duration AWs (>60%) during the recovery phase. This storm also exhibited a rapid recovery, taking only 30 hr. The Dst_c index is well-described by an exponential fit, with R1 of 0.96 and a low RMSE of 6.54 nT. However, the percentage of AWs is ∼33% throughout the recovery phase. The IMF B_Z initially remains southward during the early recovery phase but turns north during the later recovery phase, giving an average value of 0.50 nT.

Figure 1c shows a two-stage recovery storm from 23 to 28 April 2012, with few AW activity during the recovery phase. The first stage of exponential recovery is quite short, lasting only 6 hr, whereas the second stage of linear recovery is much longer, lasting about 75 hr. A single exponential fit is unable to capture the Dst_c index variation well, resulting in an R1 of 0.82 and an RMSE of 9.46 nT. However, the piece-wise fitting performs much better, resulting in an RMSE of 5.47 nT. Furthermore, few clear AWs are detected during the recovery phase, and the IMF B_Z remains predominantly southward, with a proportion of approximately 60% and an average value of −1.10 nT. Figure 1d shows a two-stage recovery storm that occurred from 26 July to 02 August 2004, with long-duration AWs almost during the entire recovery phase. Similarly, the first stage of exponential recovery is short, lasting only 16 hr, whereas the second stage of linear recovery is much longer, lasting about 97 hr. As in the

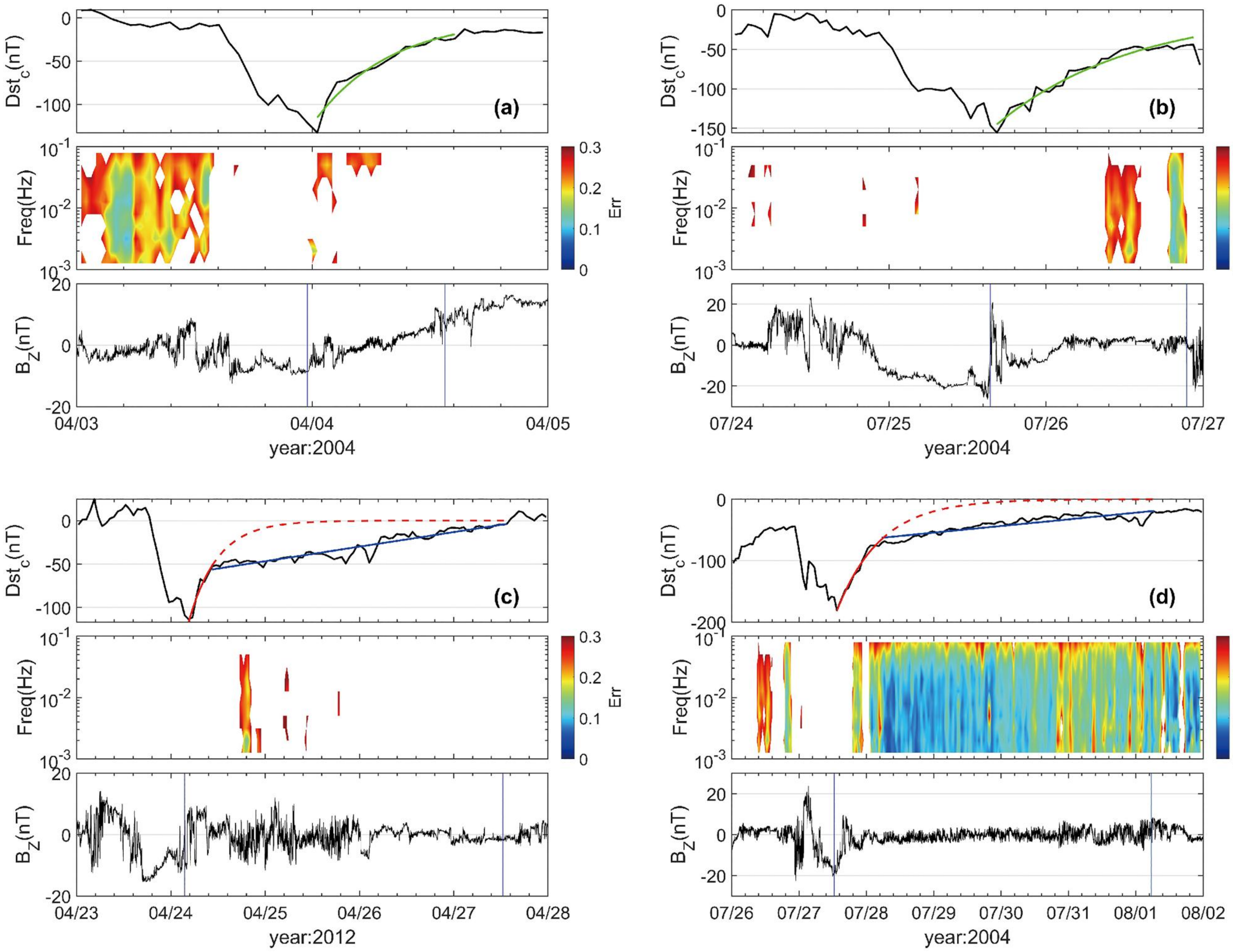

Figure 1. Four typical cases with different morphology of recovery phase and associated AWs. (a) One-stage recovery storms without AWs; (b) one-stage recovery storms with AWs; (c) two-stage recovery storms without AWs; (d) two-stage recovery storms with AWs.

previous case, a single exponential fitting is not good enough, with an R1 of 0.83 and an RMSE of 13.37 nT. However, the piece-wise fitting performance is much better, resulting in a smaller RMSE down to 6.67 nT. Furthermore, during the later recovery phase, the IMF B_Z exhibits large-amplitude Alfvénic fluctuations, with an average value of −0.13 nT. Continuous AWs are detected from 28 July to 1 August 2004 as well.

By comparing these four typical cases, it seems that a continuous southward IMF B_Z is speculated to lead to a two-stage morphology of the recovery phase.

3.2. Statistical Differences Between One-Stage and Two-Stage Recovery Storms

Table 1 presents a comparison between one-stage and two-stage recovery storms. Of the 82 isolated intense magnetic storms, approximately 41.5% (34 cases) are classified as one-stage recovery storms, while 59.5% (48 cases) are classified as two-stage recovery storms. Interestingly, the average intensity of the storm for these two categories is similar, −149 nT versus −147 nT, suggesting that the morphology of the recovery phase may be independent of storm intensity. The interplanetary origins of these 82 storms are also identified. As expected, ICME is the primary origin of intense storms, with 60 cases (73.2%) classified as ICME-driven storms. Meanwhile, 10 storms (12.2%) are classified as CIR-driven storms, and the remaining 12 storms (14.6%) are caused by complicated interplanetary origins. Compared to ICME-driven storms, CIR-driven storms are more likely to present a two-stage recovery phase. The occurrence rate of two-stage recovery storms is 70% versus 58.3%, respectively.

Table 1
Comparison of Different Recovery Types of Magnetic Storms

	One-stage	Two-stage
Number	34 (41.5%)	48 (59.5%)
Storm intensity	−149 ± 63 nT	−147 ± 50 nT
CIR-driven	3 (30%)	7 (70%)
ICME-driven	25 (41.7%)	35 (58.3%)
Others	6 (50%)	6 (50%)

Figure 2 presents the superposed epoch analysis of the Dst_c index for both one-stage recovery storms (in blue) and two-stage recovery storms (in red). The onset of the recovery phase is set as the epoch time. In general, one-stage recovery storms exhibit more rapid recovery than two-stage recovery storms. However, two-stage recovery storms recover at a notably faster rate during the early recovery phase and subsequently begin to slow down in the later recovery phase, exhibiting a distinct two-stage recovery morphology. The intersection point occurs approximately 16 hr after the epoch time.

Figure 3a shows that the storms with one-stage and two-stage recovery differ significantly in duration. More than 80% of two-stage recovery storms have a recovery phase longer than two days, while 70% of one-stage recovery storms have a duration of less than two days. To ensure equitable comparison, Figures 3b–3e exclusively illustrate the results for the later recovery phase for both types of storms. The break-point that divides the first and second parts of one-stage recovery storms is defined at the end of Section 2.2. Figures 3b and 3c show the corresponding IMF conditions during the later recovery phase. The southward IMF component, B_S, occurs more frequently in two-stage recovery storms, with an occurrence rate mostly between 0.4 and 0.6, while it is predominantly less than 0.3 for one-stage recovery storms. In contrast, the mean value of B_Z is greater than 0 nT for one-stage recovery storms and less than 0 nT for two-stage recovery storms. Figure 3d shows the occurrence rate of AWs, which are frequently observed in the later recovery phase of both types of storms. The probability of AWs for two-stage recovery storms is higher than that for one-stage recovery storms. Figure 3e presents the results specifically for cases where the occurrence rate of Alfvén waves exceeds 0.8. It is clear that the morphology of the recovery phase is influenced by the average IMF B_Z. The average IMF B_Z is predominantly southward for two-stage recovery storms, while it is mostly northward for one-stage recovery storms. Figure 3f further compares the situations of the early and later recovery phases for two-stage recovery storms. AWs are rare for the first stage of the recovery phase, with an occurrence rate of less than 20% in over 40% of the cases. For the later stage of the recovery phase, the occurrence rate of AWs is greater than 80% in over 40% of the cases. These results suggest that the IMF B_Z is crucial in determining the morphology of the recovery phase. Intense storms are classified as two-stage recovery storms when the IMF B_S dominates in the later recovery phase.

3.3. Modulation of Recovery Rate by Averaged IMF B_Z Under Different Percentages of Alfvén Waves

Here, we focus on the relationship between the averaged IMF B_Z under different percentages of AWs and the recovery rate of the Dst_c index in the later recovery phase for 48 two-stage recovery storms.

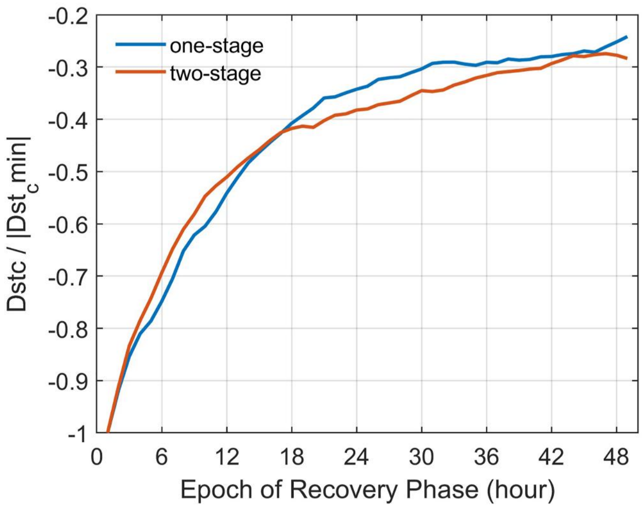

Figure 2. Superposed epoch analysis of the Dst_c index for one-stage and two-stage recovery storms.

Table 2 shows that there is a positive correlation between the average IMF B_Z and the recovery rate of the Dst_c index in the later recovery phase. The p-value provides information about the statistical significance of the linear correlation coefficient (CC). If the p-value is small (e.g., ≤0.05), it suggests that there is a statistically significant linear relationship between the variables. Interestingly, the CC increases almost linearly with the threshold value of the percentage of AWs. For example, among the 48 two-stage recovery storms, the CC is 0.55. However, when the threshold value increases to 70%, the CC for the 26 cases meeting this criterion increases to 0.90. A similar trend is obtained for the p-value, indicating that the IMF B_Z during the AWs is the primary driver of the energy input during the later recovery phase. Therefore, we can predict the morphology of the recovery phase more accurately for storms with a large percentage of AWs.

Figure 4 presents a scatter plot example from Table 2 when the percentage of AWs in the later recovery phase is larger than 70%. As previously mentioned, a nearly linear positive correlation between the average IMF B_Z and the recovery rate of the Dst_c index in the later recovery phase exists, with a CC of 0.90. When the right dot is removed, the linear correlation still exists, with a CC of 0.69. The decay of ring currents may be weakened because of the input of solar wind energy when southward IMF conditions are present during this

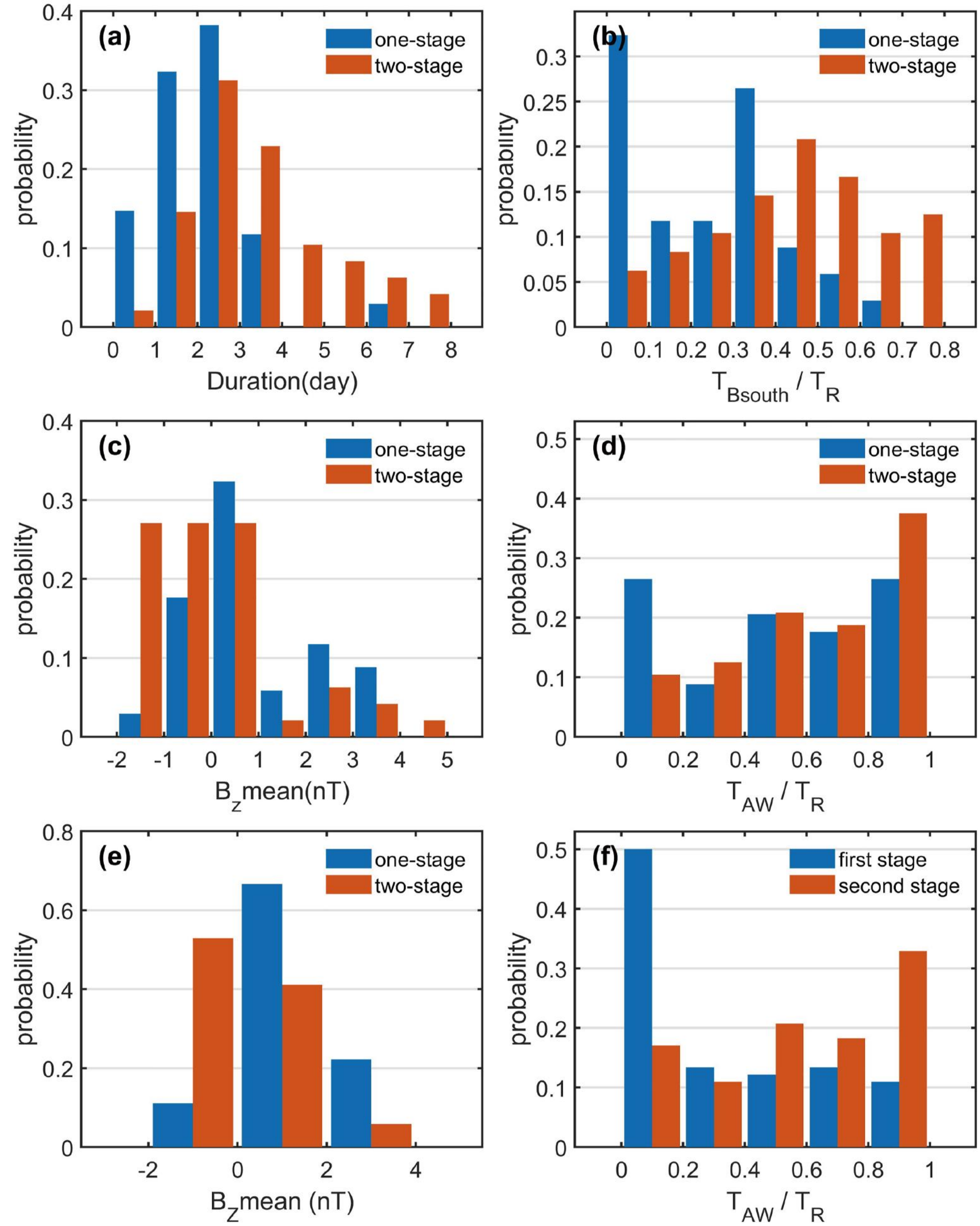

Figure 3. Differences for one-stage and two-stage recovery storms. (a) Duration of the recovery phase. (b) Incidence of the southward IMF, *Bsouth*, during the later recovery phase. (c) The average IMF B_Z during the later recovery phase. (d) Incidence of AWs in the later recovery phase. (e) The average IMF B_Z with the incidence of AWs greater than 80% in the later recovery phase. (f) Incidence of AWs during the early and later recovery phases.

period. As shown in Figure 4, when the average IMF B_Z is greater than -2 nT, the recovery rate starts to be positive, indicating the existence of a transition point when the decay process of the ring current is stronger than the growth process.

3.4. Solar Cycle Dependence

The previous results suggest that interplanetary AWs could potentially influence the recovery phase of intense magnetic storms. As interplanetary AWs demonstrate evident variability by the solar cycle, exploring the solar-cycle dependence of recovery phase morphology is pertinent. Here, we investigate isolated intense magnetic

Table 2
Correlation Between the Average IMF B_Z and the Recovery Rate of the Dst_c Index in the Later Recovery Phase for Two-Stage Recovery Storms With Different Percentages of AWs

AW percentage	Case number	CC	*p* value	Fitting slope
All cases	48	0.55	4.91×10^{-5}	3.97
>30%	44	0.64	3.46×10^{-6}	4.77
>50%	37	0.73	2.76×10^{-7}	5.91
>70%	26	0.90	4.08×10^{-10}	7.29

storms that occurred during the previous four solar cycles (cycle 21 to cycle 24) spanning from 1976 to 2019. A total of 219 intense storms are identified. Despite the challenges posed by the lack of continuous high-precision observations of solar wind plasma and interplanetary magnetic field, we successfully determine the morphology of storm recovery phase based on geomagnetic index data.

Figure 5 (a) illustrates that the smoothed monthly sunspot number (SSN) remains at a relatively high level for solar cycles 21–23, with a peak of approximately 200, before decreasing to ∼100 for solar cycle 24. The number of intense magnetic storms exhibits a similar pattern across these four solar cycles, decreasing from more than 60 to approximately 20. Moreover, the proportion of two-stage recovery storms exceeds 60% in these four solar cycles, reaching a peak of 82% during solar cycle 22, as illustrated in Figure 5b. Additionally, both the number and the percentage of storms exhibiting a two-stage recovery are categorized into the four phases of the solar cycle, as shown in Figures 5c and 5d. The onsets of the phases of the solar cycle are determined by the following method: When the difference between the monthly SSN and the average SSN during a whole solar cycle is greater or less than the standard deviation of the SSN in this solar cycle, the onset of solar maximum or minimum is declared. The ascending and declining phases are located between the maximum and the minimum. A strong trend in the number of intense storms is observed, with a minimum during solar minimum and a maximum during solar maximum, consistent with the ejecta presented by Xu & Borovsky (2015). Additionally, the percentage of two-stage recovery storms peaks during solar minimum. This may be attributed to the prevalence of high-speed streamers from coronal holes with abundant AWs during the solar minimum, which could easily lead to two-phase recovery phases.

3.5. Monthly Distribution of Storms and Origins of Alfvén Waves

The monthly distribution of one-stage and two-stage recovery storms are shown in Figures 6a and 6b. One-stage recovery storms are more prevalent during October and November; while two-stage recovery storms are more prevalent during March and May and during August and October. The Russell-McPherron effect results in heightened geomagnetic disturbances around the vernal equinox (March 21) and the autumnal equinox (September 23) (McPherron et al., 2009). Our study focuses on intense magnetic storms, which are predominantly caused by transient ICME events. Nevertheless, there is statistical signature of the Russell-McPherron effect for both two types of storms. Besides, the signature is more clear for the two-stage recovery storms.

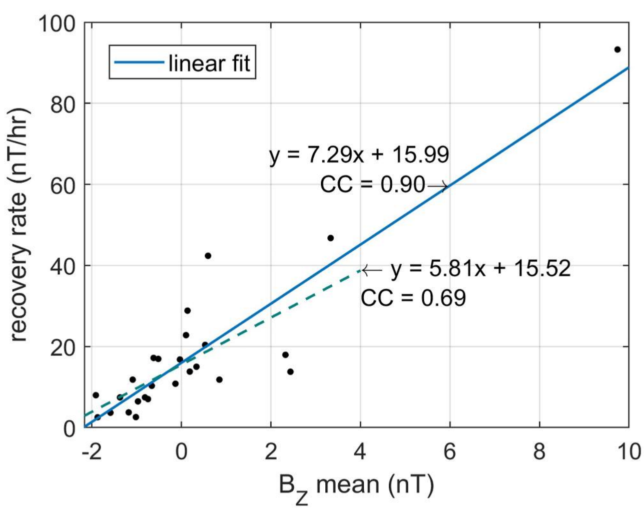

Figure 4. Scatter plot of the average IMF B_Z and the recovery rate of the Dst_c index in the later recovery phase, with the CC of 0.90. When the right dot is removed, the fitting result is shown by the dashed line.

By using the technique proposed by Li et al. (2020), we classify the solar wind plasma during the later recovery phase into three types: coronal-hole-origin plasma (CHOP), streamer-belt-origin plasma (SBOP), and ejecta (EJECT). As shown in Figure 6c, one of the dominant sources of solar wind during the later recovery phase is SBOP. The difference between the two types of storms lies in the fact that one-stage recovery storms have a higher proportion of EJECT, while two-stage recovery storms have a higher proportion of CHOP. In general, CHOP exhibits stronger Alfvénicity. This suggests that solar wind from coronal holes is more likely to contribute to the occurrence of a two-stage recovery storm. As shown in Figure 6d, approximately 80% of Alfvén Waves originate from CHOP and SBOP types of solar wind and the dominant source is CHOP for two-stage recovery storms. This result provides the solar wind sources of Alfvén waves that control the later recovery of geomagnetic storms.

4. Discussion and Conclusion

The recovery phase of intense magnetic storms is influenced by several factors. During the early recovery phase, rapid decay of the ring current is caused by convective drift loss out of the dayside magnetopause (Liemohn et al., 1999). In the later recovery phase, the symmetric ring current predominantly contributes to the recovery but does so much more slowly due to

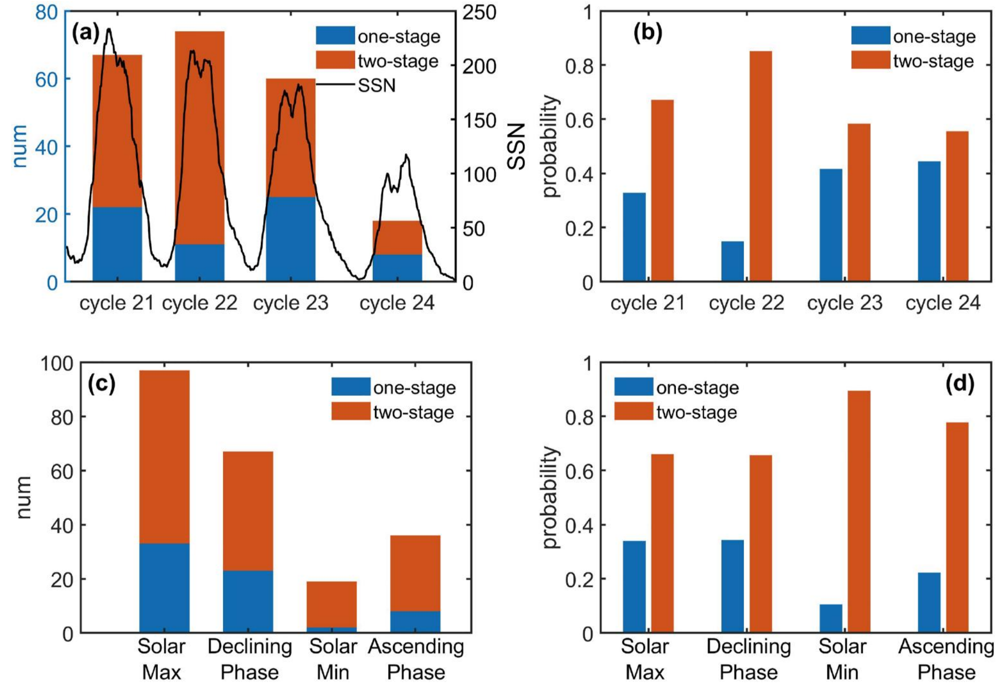

Figure 5. Solar cycle dependence of recovery phase morphology of intense magnetic storms.

the dominant charge-exchange contribution (Ebihara & Ejiri, 2000). As a result, the recovery phase morphology may consist of two stages due to the different decay mechanisms of the ring current. Previous studies have reported that the recovery rate of the *Dst* index remains constant and depends on the storm intensity (Choraghe et al., 2021). Telloni et al. (2021) confirmed that the duration of the recovery phase is directly proportional to the

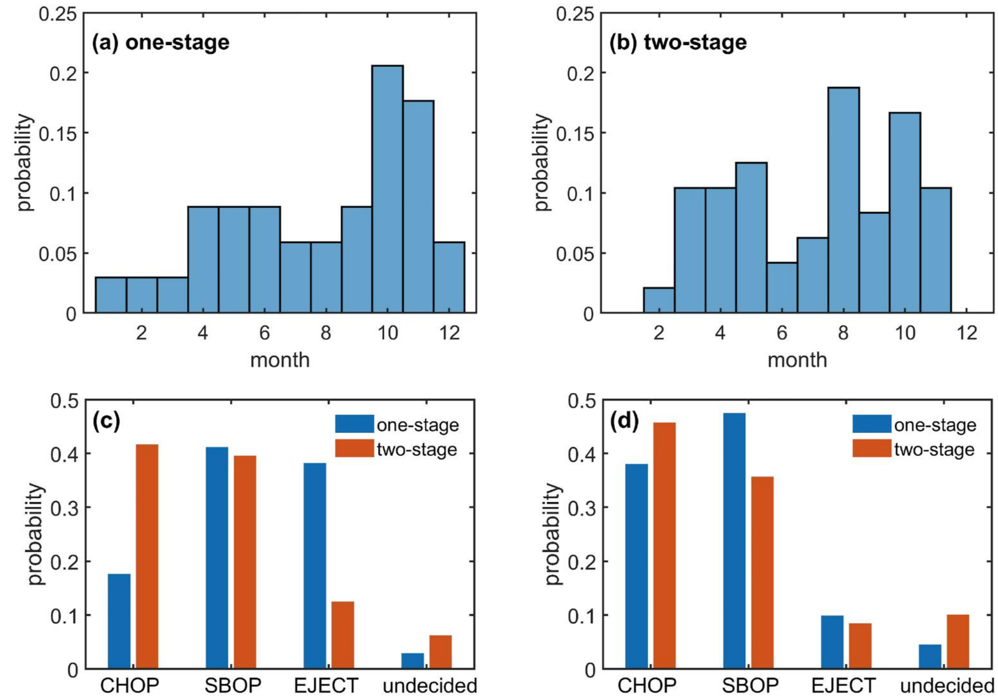

Figure 6. Monthly Distribution of Storms, (a) one-stage recovery storms; (b) two-stage recovery storms. (c) The origin of solar wind during the later recovery phase; (d) the origin of Alfvénic solar wind during the later recovery phase.

duration of AWs. Nonetheless, the recovery phase morphology and the corresponding impact factors in the solar wind are rarely discussed in the literature.

In this study, we conduct a statistical survey of 82 isolated intense magnetic storms that occurred from 1995 to 2020 and focus on the characteristics of the recovery phase morphology. In general, intense storms can be classified into two types: one-stage recovery storms with a rapid exponential recovery, and two-stage recovery storms with a piece-wise recovery, a rapid exponential recovery in the early recovery phase and a slow linear recovery in the later recovery phase. During the last two solar cycles, two-stage recovery storms are more dominant than one-stage recovery storms, with an occurrence rate of 60% versus 40%. Interestingly, during solar minimum, the occurrence rate of two-stage recovery storms increased to 89%. This may be attributed to the prevalence of high-speed streams from coronal holes with abundant AWs. On the basis of the superposed epoch analysis, we found that two-stage recovery storms recover much more rapidly in the early recovery phase, but begin to slow down in the later recovery phase. The southward IMF associated with AWs plays a critical role in shaping the recovery phase morphology. For two-stage recovery storms, the occurrence rate and mean value of the southward IMF and the incidence of AWs are significantly higher than those of one-stage recovery storms. Moreover, during the later recovery phase, we observe a nearly linear correlation between the decay rate of the *Dst* index and the amplitude of the IMF B_Z when the solar wind exhibits a high degree of Alfvénicity. Geomagnetic storms that undergo one-stage recovery show a greater portion of EJECT, while those that undergo two-stage recovery exhibit a higher proportion of CHOP. This observation suggests that the sources of Alfvén waves in the solar wind play a crucial role in controlling the recovery morphology of geomagnetic storms.

Appendix A: Case List

T_{start} is the start time of the recovery phase; T_{end} is the end time of the recovery phase; R1 and R2 are introduced in Section 2; R3 is the best goodness by using a piece-wise function, which is calculated in the same way as R1; k is the slope of the linear fit in the later recovery phase; τ_1 is the decay constant of the exponential fit in the early recovery phase; τ_2 is the decay constant of the exponential fit for the whole recovery phase; flag indicates the recovery type of storms, 1 for one-stage recovery storms, and 2 for two-stage recovery storms (Table A1).

The fitting model is as follows:

$$Dst_c = A \times e^{-t/\tau_2} \tag{A1}$$

$$Dst_c = \begin{cases} B \times e^{-t/\tau_1}, & t < t_{cp} \\ k \times (t - t_c) + C, & t \geq t_{cp} \end{cases} \tag{A2}$$

where A, B and C are parameters associated with the intensity of magnetic storm, t is the time from the start of recovery phase, t_c is charging point between early recovery phase and later recovery phase.

Table A1
The Goodness of Fitting and Fitting Parameter

T_{start}	T_{end}	R1	R2	R3	k	τ_1	τ_2	Flag
3/26/95 17:30	3/29/95 0:30	0.521	−1.653	0.870	9.788	13.216	60.173	2
4/7/95 18:30	4/13/95 2:30	0.722	−1.052	0.931	7.449	19.826	90.773	2
9/27/95 20:30	9/29/95 8:30	0.835	−0.434	0.971	49.076	10.792	28.963	2
10/19/95 6:30	10/19/95 18:30	0.988	0.988	0.989	99.335	11.571	11.443	1
10/23/96 4:30	10/26/96 17:30	0.614	−1.854	0.925	7.031	9.121	68.014	2
4/21/97 23:30	4/23/97 3:30	0.927	0.910	0.976	25.802	18.546	21.364	1
5/15/97 12:30	5/18/97 13:30	0.750	0.673	0.931	9.037	32.029	44.908	2
10/11/97 3:30	10/14/97 1:30	0.662	−0.128	0.938	7.437	15.801	46.716	2
11/7/97 4:30	11/9/97 9:30	0.879	0.816	0.983	0.440	15.347	21.349	2
11/23/97 12:30	11/26/97 2:30	0.939	0.891	0.973	16.730	28.005	35.773	1
2/18/98 0:30	2/20/98 9:30	0.765	0.663	0.931	−9.379	18.580	27.996	2
3/10/98 20:30	3/17/98 8:30	0.504	−1.487	0.822	2.542	23.803	135.170	2
5/4/98 5:30	5/7/98 22:30	0.804	0.213	0.951	23.183	14.543	41.679	2
8/6/98 11:30	8/9/98 10:30	0.956	0.677	0.968	31.387	19.215	33.730	2
8/27/98 9:30	9/1/98 6:30	0.766	0.510	0.925	2.584	34.673	64.564	2
9/25/98 9:30	9/28/98 6:30	0.795	0.552	0.975	14.883	12.295	27.054	2
10/19/98 15:30	10/23/98 12:30	0.674	−1.085	0.842	11.821	20.842	77.051	2
11/8/98 6:30	11/8/98 18:30	0.972	0.941	0.985	163.684	12.566	10.535	1
11/9/98 18:30	11/12/98 6:30	0.939	0.756	0.977	19.091	17.629	28.579	2
1/13/99 23:30	1/16/99 22:30	0.932	0.818	0.956	19.281	27.836	39.685	1
2/18/99 17:30	2/21/99 12:30	0.961	0.939	0.973	15.267	40.608	34.602	1
9/22/99 23:30	9/25/99 4:30	0.957	0.923	0.992	29.036	17.263	21.696	1
10/22/99 6:30	10/29/99 15:30	0.501	−0.289	0.879	3.747	13.533	87.414	2
7/16/00 0:30	7/18/00 19:30	0.946	0.718	0.969	46.755	12.851	24.134	2
8/12/00 9:30	8/14/00 21:30	0.963	0.934	0.986	35.908	17.694	22.045	1
9/17/00 23:30	9/21/00 19:30	0.828	0.682	0.954	22.800	16.936	31.300	2
10/5/00 13:30	10/8/00 10:30	0.960	0.928	0.989	20.998	17.715	22.602	1
10/14/00 14:30	10/15/00 19:30	0.958	0.953	0.978	39.644	17.398	18.814	1
10/29/00 3:30	10/31/00 4:30	0.961	0.961	0.966	20.395	26.573	27.257	1
11/6/00 21:30	11/8/00 9:30	0.953	0.906	0.968	52.307	26.665	21.119	1
11/29/00 13:30	11/30/00 23:30	0.867	0.481	0.951	42.375	14.431	25.766	2
3/20/01 13:30	3/22/01 10:30	0.944	0.856	0.986	37.787	17.021	23.519	1
4/11/01 23:30	4/13/01 10:30	0.970	0.925	0.989	65.273	13.834	17.475	1
4/18/01 6:30	4/19/01 18:30	0.920	0.283	0.975	57.302	10.374	22.414	2
4/22/01 15:30	4/24/01 21:30	0.893	0.767	0.939	13.769	46.783	31.969	2
8/17/01 21:30	8/18/01 17:30	0.931	0.637	0.967	93.273	10.800	16.701	2
10/28/01 11:30	10/31/01 12:30	0.951	0.749	0.976	27.806	21.975	35.594	2
11/1/01 10:30	11/3/01 2:30	0.941	0.865	0.964	20.597	20.296	26.612	1
11/6/01 6:30	11/12/01 8:30	0.947	0.938	0.985	3.550	30.011	34.953	1
11/24/01 16:30	11/28/01 7:30	0.979	0.957	0.985	24.476	24.187	29.399	1
3/24/02 20:30	3/25/02 15:30	0.846	−0.496	0.938	54.160	159.938	24.380	2
4/20/02 8:30	4/23/02 4:30	0.889	0.802	0.971	11.821	22.483	32.282	2
5/11/02 19:30	5/13/02 12:30	0.945	0.786	0.981	28.844	16.977	25.120	2

Table A1
Continued

5/23/02 17:30	5/25/02 23:30	0.925	0.911	0.960	−1.700	21.055	24.329	1
8/2/02 5:30	8/3/02 17:30	0.636	−3.412	0.818	19.771	9.181	45.842	2
8/21/02 6:30	8/22/02 17:30	0.882	0.876	0.943	18.420	23.950	23.641	2
9/4/02 5:30	9/6/02 9:30	0.952	0.917	0.981	25.483	24.305	29.622	1
9/8/02 0:30	9/15/02 6:30	0.546	−0.865	0.841	7.985	26.427	129.403	2
11/21/02 10:30	11/26/02 19:30	0.586	−2.515	0.864	3.664	24.009	132.133	2
5/29/03 23:30	6/1/03 10:30	0.899	0.599	0.984	32.031	10.731	22.897	2
6/18/03 9:30	6/20/03 7:30	0.960	0.896	0.981	34.698	19.550	25.489	1
7/12/03 5:30	7/14/03 10:30	0.834	−0.944	0.956	16.939	9.729	37.540	2
10/30/03 22:30	11/3/03 6:30	0.951	0.946	0.973	11.950	9.653	10.995	1
4/4/04 0:30	4/4/04 14:30	0.945	0.872	0.958	104.283	5.821	7.771	1
7/25/04 16:30	7/26/04 22:30	0.960	0.953	0.977	14.742	19.256	20.965	1
7/27/04 13:30	8/1/04 6:30	0.829	0.211	0.958	14.756	14.228	61.542	2
8/30/04 22:30	9/2/04 1:30	0.941	0.939	0.951	10.822	15.543	48.180	2
11/10/04 10:30	11/16/04 3:30	0.780	−0.047	0.967	11.052	21.906	23.213	1
5/8/05 18:30	5/11/05 2:30	0.781	0.362	0.936	17.176	15.335	32.755	2
5/15/05 8:30	5/19/05 20:30	0.839	0.401	0.980	16.370	14.120	40.682	2
5/30/05 13:30	5/31/05 21:30	0.928	0.902	0.951	22.956	27.339	23.272	1
6/13/05 0:30	6/14/05 13:30	0.969	0.969	0.974	11.304	22.629	22.431	1
8/24/05 11:30	8/28/05 7:30	0.871	0.701	0.983	13.803	16.070	30.511	2
8/31/05 19:30	9/7/05 1:30	0.569	−1.495	0.868	6.458	21.703	123.734	2
8/6/11 3:30	8/9/11 14:30	0.757	−0.059	0.964	7.123	16.289	49.036	2
10/25/11 1:30	10/28/11 15:30	0.876	0.799	0.977	17.939	22.427	32.778	2
4/24/12 4:30	4/27/12 13:30	0.816	−0.525	0.938	16.787	7.366	40.168	2
7/15/12 16:30	7/19/12 5:30	0.952	0.934	0.956	23.499	33.426	38.579	1
10/1/12 4:30	10/3/12 4:30	0.905	0.856	0.974	26.466	16.438	21.501	1
10/9/12 8:30	10/11/12 22:30	0.869	0.260	0.947	15.004	17.964	39.244	2
11/14/12 7:30	11/16/12 10:30	0.933	0.871	0.985	13.710	11.967	16.943	1
3/17/13 20:30	3/22/13 2:30	0.407	−0.505	0.883	1.470	10.393	66.406	2
6/1/13 8:30	6/3/13 19:30	0.938	0.716	0.977	20.388	17.232	29.061	2
6/29/13 6:30	7/1/13 22:30	0.911	0.876	0.974	12.143	24.781	30.955	1
3/17/15 22:30	3/22/15 3:30	0.824	−0.118	0.976	16.797	14.201	51.374	2
6/23/15 4:30	6/29/15 11:30	0.782	−0.020	0.928	9.212	22.173	75.207	2
10/7/15 22:30	10/11/15 9:30	0.720	−1.172	0.881	10.302	11.495	57.419	2
12/20/15 22:30	12/23/15 5:30	0.952	0.951	0.977	19.696	24.012	24.318	1
1/1/16 0:30	1/2/16 6:30	0.939	0.937	0.967	24.433	17.798	17.634	1
10/13/16 23:30	10/14/16 19:30	0.943	0.830	0.966	62.737	21.039	14.726	1
5/28/17 7:30	5/29/17 1:30	0.957	0.946	0.993	128.642	11.882	12.857	1
8/26/18 6:30	8/31/18 4:30	0.845	0.277	0.961	11.280	14.628	45.973	2

Data Availability Statement

Publicly available data sets were analyzed in this study. The OMNI data and the Wind data from https://cdaweb.gsfc.nasa.gov/pub/data/wind/; Dst data from https://wdc.kugi.kyoto-u.ac.jp/.

Journal of Geophysical Research: Space Physics 10.1029/2023JA032057

Acknowledgments

This work is supported by NNSFC grants (42022032, 42374198, 41874203, 42188101), project of Civil Aerospace "13th Five Year Plan" Preliminary Research in Space Science (D020301, D030202), Strategic Priority Research Program of CAS (Grant No. XDA17010301) and Key Research Program of Frontier Sciences CAS (Grant No. QYZDJ-SSW-JSC028). H. Li is also supported by the International Partnership Program of CAS (Grant No. 183311KYSB20200017) and in part by the Specialized Research Fund for State Key Laboratories of China.

References

Aguado, J., Cid, C., Saiz, E., & Cerrato, Y. (2010). Hyperbolic decay of the dst index during the recovery phase of intense geomagnetic storms: Hyperbolic decay of the dst index. *Journal of Geophysical Research*, *115*(A7). A07220. https://doi.org/10.1029/2009JA014658

Akasofu, S.-I., Chapman, S., & Venkatesan, D. (1963). The main phase of great magnetic storms. *Journal of Geophysical Research (1896-1977)*, *68*(11), 3345–3350. https://doi.org/10.1029/jz068i011p03345

Burton, R. K., McPherron, R. L., & Russell, C. T. (1975). An empirical relationship between interplanetary conditions and *dst*. *Journal of Geophysical Research*, *80*(31), 4204–4214. https://doi.org/10.1029/ja080i031p04204

Choraghe, K., Raghav, A., Chakrabarty, D., Kasthurirangan, S., & Bijewar, N. (2021). Properties of the recovery phase of extreme storms. *Journal of Geophysical Research: Space Physics*, *126*(9). e2020JA028685. https://doi.org/10.1029/2020ja028685

D'Amicis, R., Matteini, L., Bruno, R., & Velli, M. (2020). Large amplitude fluctuations in the alfvénic solar wind. *Solar Physics*, *295*(3), 46. https://doi.org/10.1007/s11207-020-01606-2

Denton, M. H., Borovsky, J. E., Skoug, R. M., Thomsen, M. F., Lavraud, B., Henderson, M. G., et al. (2006). Geomagnetic storms driven by icme- and cir-dominated solar wind. *Journal of Geophysical Research*, *111*(A7), A07S07. https://doi.org/10.1029/2005JA011436

Dessler, A. J., & Parker, E. N. (1959). Hydromagnetic theory of geomagnetic storms. *Journal of Geophysical Research*, *64*(12), 2239–2252. https://doi.org/10.1029/jz064i012p02239

Ebihara, Y., & Ejiri, M. (2000). Simulation study on fundamental properties of the storm-time ring current. *Journal of Geophysical Research*, *105*(A7), 15843–15859. https://doi.org/10.1029/1999ja900493

Feldstein, Y. I., Dremukhina, L. A., Mall, U., & Woch, J. (2000). On the two-phase decay of the dst-variation. *Geophysical Research Letters*, *27*(17), 2813–2816. https://doi.org/10.1029/2000gl003783

Gonzalez, W. D., Joselyn, J. A., Kamide, Y., Kroehl, H. W., Rostoker, G., Tsurutani, B. T., & Vasyliunas, V. M. (1994). What is a geomagnetic storm? *Journal of Geophysical Research*, *99*(A4), 5771–5792. https://doi.org/10.1029/93ja02867

Gonzalez, W. D., Tsurutani, B. T., & Clúa de Gonzalez, A. L. (1999). Interplanetary origin of geomagnetic storms. *Space Science Reviews*, *88*(3–4), 529–562. https://doi.org/10.1023/a:1005160129098

Hamilton, D. C., Gloeckler, G., Ipavich, F. M., Stüdemann, W., Wilken, B., & Kremser, G. (1988). Ring current development during the great geomagnetic storm of february 1986. *Journal of Geophysical Research*, *93*(A12), 14343–14355. https://doi.org/10.1029/ja093ia12p14343

Khanal, K., Adhikari, B., Chapagain, N. P., & Bhattarai, B. (2019). Hildcaa-related gic and possible corrosion hazard in underground pipelines: A comparison based on wavelet transform. *Space Weather*, *17*(2), 238–251. https://doi.org/10.1029/2018SW001879

Kozyreva, O. V., Pilipenko, V. A., Belakhovsky, V. B., & Sakharov, Y. A. (2018). Ground geomagnetic field and gic response to march 17, 2015, storm. *Earth Planets and Space*, *70*(1), 157. https://doi.org/10.1186/s40623-018-0933-2

Lei, J., Huang, F., Chen, X., Zhong, J., Ren, D., Wang, W., et al. (2018). Was magnetic storm the only driver of the long-duration enhancements of daytime total electron content in the asian-australian sector between 7 and 12 september 2017? *Journal of Geophysical Research: Space Physics*, *123*(4), 3217–3232. https://doi.org/10.1029/2017ja025166

Li, H., Wang, C., Chao, J., & Hsieh, W. (2016). A new approach to identify interplanetary alfvén waves and to obtain their frequency properties. *Journal of Geophysical Research: Space Physics*, *121*(1), 42–55. https://doi.org/10.1002/2015ja021749

Li, H., Wang, C., Tu, C., & Xu, F. (2020). Machine learning approach for solar wind categorization. *Earth and Space Science*, *7*(5). e2019EA000997. https://doi.org/10.1029/2019EA000997

Li, Q., Zhang, R., Liu, L., Kuai, J., Yang, N., Zhong, J., et al. (2022). Persistent eastward EEJ enhancement during the geomagnetic storm recovery phases. *Journal of Geophysical Research: Space Physics*, *127*(5). e2022JA030258. https://doi.org/10.1029/2022ja030258

Liemohn, M. W., Kozyra, J. U., Jordanova, V. K., Khazanov, G. V., Thomsen, M. F., & Cayton, T. E. (1999). Analysis of early phase ring current recovery mechanisms during geomagnetic storms. *Geophysical Research Letters*, *26*(18), 2845–2848. https://doi.org/10.1029/1999GL900611

McPherron, R., Baker, D., & Crooker, N. (2009). Role of the russell–mcpherron effect in the acceleration of relativistic electrons. *Journal of Atmospheric and Solar-Terrestrial Physics*, *71*(10–11), 1032–1044. https://doi.org/10.1016/j.jastp.2008.11.002

O'Brien, T. P., & McPherron, R. L. (2000). An empirical phase space analysis of ring current dynamics: Solar wind control of injection and decay. *Journal of Geophysical Research*, *105*(A4), 7707–7719.

Raghav, A. N., Choraghe, K., & Shaikh, Z. I. (2019). The cause of an extended recovery from an ICME-induced extreme geomagnetic storm: A case study. *Monthly Notices of the Royal Astronomical Society*, *488*(1), 910–917.

Raghav, A. N., & Kule, A. (2018). The first in situ observation of torsional alfvén waves during the interaction of large-scale magnetic clouds. *Monthly Notices of the Royal Astronomical Society: Letters*, *476*(1), L6–L9. https://doi.org/10.1093/mnrasl/sly020

Telloni, D., D'Amicis, R., Bruno, R., Perrone, D., Sorriso-Valvo, L., Raghav, A. N., & Choraghe, K. (2021). Alfvénicity-related long recovery phases of geomagnetic storms: A space weather perspective. *The Astrophysical Journal*, *916*(2), 64. https://doi.org/10.3847/1538-4357/ac071f

Tsurutani, B. T., & Gonzalez, W. D. (1987). The cause of high-intensity long-duration continuous ae activity (HILDCAAS): Interplanetary alfvén wave trains. *Planetary and Space Science*, *35*(4), 405–412. https://doi.org/10.1016/0032-0633(87)90097-3

Xu, F., & Borovsky, J. E. (2015). A new four-plasma categorization scheme for the solar wind: 4-plasma solar-wind categorization. *Journal of Geophysical Research: Space Physics*, *120*(1), 70–100. https://doi.org/10.1002/2014JA020412

Yermolaev, Y. I., Lodkina, I. G., Nikolaeva, N. S., & Yermolaev, M. Y. (2014). Influence of the interplanetary driver type on the durations of the main and recovery phases of magnetic storms. *Journal of Geophysical Research: Space Physics*, *119*(10), 8126–8136. https://doi.org/10.1002/2014ja019826

Yokoyama, N., & Kamide, Y. (1997). Statistical nature of geomagnetic storms. *Journal of Geophysical Research*, *102*(A7), 14215–14222. https://doi.org/10.1029/97ja00903

Zhang, X.-Y., Moldwin, M. B., Steinberg, J. T., & Skoug, R. M. (2014). Alfvén waves as a possible source of long-duration, large-amplitude, and geoeffective southward imf: Zhang et al. *Journal of Geophysical Research: Space Physics*, *119*(5), 3259–3266. https://doi.org/10.1002/2013JA019623